Numerical Modeling of Helical Flow of Viscoplastic Fluids in Eccentric Annuli

Q. E. Hussain and M. A. R. Sharif
Dept. of Aerospace Engineering and Mechanics, The University of Alabama, Tuscaloosa, AL 35487

Helical flow of viscoplastic Herschel-Bulkley fluids in concentric and eccentric annuli with rotating inner cylinder was investigated numerically. Similar flows occur in drilling operations of oil and gas wells. A finite volume algorithm with a nonstaggered grid system and a nonorthogonal curvilinear coordinate system to handle irregular geometry of an eccentric annulus was used to analyze the problem. Papanastasiou's modification of the Herschel-Bulkley (Yield-Power-Law) constitutive equation was used to model the shear rate-dependent viscosity of a viscoplastic fluid. For a fixed axial pressure gradient, the axial flow rate increased with increasing rotational speed of the inner cylinder. The discharge, as well as torque required to rotate the inner pipe, increased with increasing eccentricity for a fixed axial pressure gradient and inner cylinder rotational speed. Discharge also increased with increasing axial pressure gradient at a fixed eccentricity and rotational speed of the inner pipe. The flow field in an eccentric annulus is complex because vigorous secondary flow is produced in addition to the primary axial helical flow. Blockage at the narrow part of the eccentric annulus, when present, intensifies this secondary flow, with the discharge decreasing initially, then increasing, and decreasing again with increasing height of the blockage.

Introduction

Axial flow in an annular space with a rotating inner or outer cylinder is known as helical flow since the fluid particles move in helical paths. Helical flows are encountered in many engineering applications such as the flow of drilling fluid in well-bore. During drilling for oil wells, drilling-fluid circulates through the annular space between the rotating drill shaft and the fixed well-bore to remove the cuttings. The drilling fluid is typically a viscoplastic fluid of pseudoplastic nature whose viscosity decreases with increasing shear rate. In industry, it is a common practice to neglect the effect of the drill-pipe rotation for the design of the drilling process. This assumption simplifies the flow problem significantly, and it has been solved by various investigators in concentric and eccentric annulus including the effect of a partial blockage (Haciislamoglu and Langlinais, 1990; Azouz et al., 1993; Hussain and Sharif, 1997, 1998). However, the number of studies taking into account the effect of inner or outer cylinder rotation is very limited even in the relatively simple case of a concentric annulus.

The fundamental theory for concentric helical flow was given by Coleman and Noll (1959) for a general fluid. There are some works available involving nonviscoplastic fluids (Bird et al., 1987; Dostal et al., 1993; Batra and Eissa, 1994) and viscoplastic fluids (Bhattacharya and Javadpour, 1992) in a concentric annulus.

Under directional or inclined drilling condition gravity pulls the drill shaft downwards causing the annulus to become eccentric. This changes the flow geometry, and the cylindrical coordinate system cannot be used to define it. Consequently, the flow analysis becomes more complex and analytical techniques fall short of handling this added complexity. There is a severe shortage of literature which takes into account the eccentricity of the annulus in helical flow. Beverly and Tanner (1992) have studied this problem for Bingham plastics using a biviscosity rheological model and finite-element method. Hai-Qiao and Ji-Zhou (1994) have used an approximate analytical method which they refer to as an infinite subdivision method to study power-law and Bingham plastic flu-

Correspondence concerning this article should be addressed to M. A. R. Sharif.
Current address of Q. E. Hussain: AP Automotive Systems, Inc., 543 Matzinger Road, Toledo, OH 43612.

ids in eccentric annulus. This type of flow was numerically studied by Cui and Liu (1995) for power-law fluids. They used stream function-axial velocity formulation in a bipolar coordinate system. This results in a biharmonic equation rendering the solution process to be inherently difficult. A simplistic procedure was undertaken by Wei et al. (1998) involving power-law fluids in eccentric annulus. They formulated a hybrid-analytical solution based on a concentric annulus solution for an eccentric case using a constant inner pipe radius and a variable radius for the outer pipe to account for the eccentricity. They wrongfully assumed the flow to be symmetric across the plane of geometrical symmetry. Such solutions may be useful for field application where a rough estimate of frictional pressure drop is often what is needed, but it fails to provide valuable information about the flow physics. Neither of these works is capable of handling any geometric irregularities such as a partial blockage which is often caused by cutting deposition.

The above discussion suggests that there is only a handful of works available in a helical flow of viscoplastic fluids in concentric or eccentric annulus and none of these studies take the effect of a blockage into account. In this study nonorthogonal curvilinear coordinates with nonstaggered or collocated grid has been used to investigate the helical flow of viscoplastic fluids in concentric, eccentric, as well as irregular eccentric annulus due to the presence of a blockage. A primitive variable velocity and pressure based algorithm has been used in the computation unlike any of the previous works. The effects of the rotational speed of the inner pipe, eccentricity, blockage height on the total discharge, and the torque requirement for rotating the inner cylinder is investigated. The developed numerical model, as well as the predicted results in particular, can be used in planning oil and gas well drilling operations.

Governing Equations

The geometry of the annular flow and the coordinate system used in the computation is shown in Figure 1. A cross-sectional view of the partially blocked eccentric annulus is shown in Figure 2. The flow is considered fully developed in the axial (z) direction. Thus, the flow is essentially two-dimensional (2-D) in the cross-sectional (xy) plane. The general conservation equation can be written as

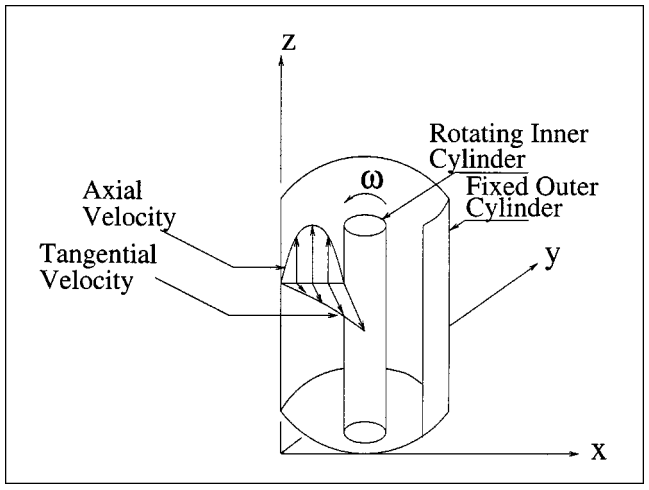

Figure 1. Flow configuration and coordinate system.

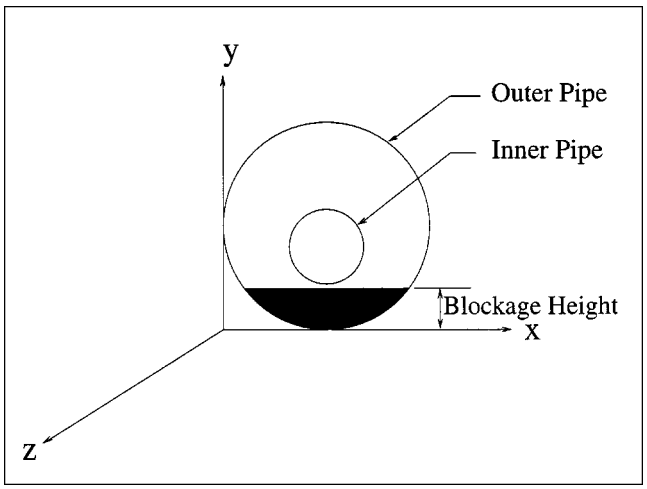

Figure 2. Flow geometry with blockage.

$$\frac{\partial}{\partial x}(\rho u\phi)+\frac{\partial}{\partial y}(\rho v\phi)=\frac{\partial}{\partial x}\left(\Gamma\frac{\partial\phi}{\partial x}\right)+\frac{\partial}{\partial y}\left(\Gamma\frac{\partial\phi}{\partial y}\right)+S \quad (1)$$

where the general variable ϕ can be u, v, or w. The diffusion coefficient is denoted by Γ, and S is the source term. For the mass conservation equation, $\phi=1$, $\Gamma=0$, and $S=0$. The axial velocity component w is solved as a scalar. The specified constant axial pressure gradient $dp/dz=\tilde{P}$ enters into the system as a source term in the equation for the w velocity component. The source terms for the u and v momentum equations are $-\partial p/\partial x$ and $-\partial p/\partial y$, respectively. The pressure in the cross-sectional plane is variable, but its gradient in the axial direction is constant for fully developed flow.

The second invariant of the rate of deformation tensor, or, the shear rate for this flow is obtained as (Bird et al., 1960)

$$\dot{\gamma}=\left[2\left(\frac{\partial u}{\partial x}\right)^2+2\left(\frac{\partial v}{\partial y}\right)^2+\left(\frac{\partial v}{\partial x}+\frac{\partial u}{\partial y}\right)^2+\left(\frac{\partial w}{\partial x}\right)^2+\left(\frac{\partial w}{\partial y}\right)^2\right]^{1/2}. \quad (2)$$

According to the yield-power-law rheological model, the shear stress and the shear rate are related by the following expression

$$\tau=\tau_y+K\dot{\gamma}^n \quad \text{for } |\tau|>\tau_y$$
$$\dot{\gamma}=0 \quad \text{for } |\tau|\le\tau_y \quad (3)$$

where K and n are the plastic viscosity ($\text{Pa}\cdot\text{s}^n$) and the flow behavior index, respectively. Bingham plastic is a special case

of this model for $n=1$. When the shear stress τ (Pa) falls below the yield stress τ_y (Pa), a solid structure (unyielded region) is formed in yield-power-law fluids. A viscoplastic fluid does not have a constant viscosity like a Newtonian fluid. However, in numerical modeling, the concept of viscosity is used for viscoplastic fluids to make the analysis analogous to Newtonian fluids. This viscosity, known as the apparent viscosity, is obtained as

$$\mu_a = \frac{\tau}{\dot{\gamma}}. \tag{4}$$

The yield-power-law rheological model for viscoplastic fluids described by Eq. 3 will encounter a singularity problem for vanishingly small shear rate in the unyielded region while calculating the apparent viscosity. This is the most difficult aspect of numerical modeling of fluids with yield stress. Beverly and Tanner (1992) and Vradis et al. (1993) overcame this problem using the biviscosity model in which the apparent viscosity is ''frozen'' at a certain high level when the shear rate falls below a certain low level. Azouz et al. (1993) used a minimum cutoff value of the shear rate. The difficulty associated with these methods involves the determination of the cutoff minimum shear rate and maximum viscosity for which considerable numerical experimentation is required. Papanastasiou (1987) proposed a constitutive equation for fluids with yield stress, where a material parameter controls the exponential growth of stress which is valid for both yielded and unyielded regions. In 1-D flow, Papanastasiou's modification to the yield-power-law model becomes

$$\tau = \tau_y\left[1 - e^{-m\dot{\gamma}}\right] + K\dot{\gamma}^n \tag{5}$$

where m is the stress growth exponent(s). This model is empirical in nature and is designed primarily to offer a convenient constitutive equation for numerical simulation. It closely mimics the shear stress vs. shear rate curves for ideal Bingham plastics for $m \geq 100$ s (Ellwood et al., 1990). It has been successfully implemented in numerical modeling of different viscoplastic and yield-power-law fluid flow by Ellwood et al. (1990), Abdali et al. (1992), Mitsoulis et al. (1993), Pham and Mitsoulis (1994), and Hussain and Sharif (1997, 1998). The shear stress value obtained from Eq. 5 is divided by the shear rate calculated from Eq. 2 to obtain the apparent viscosity everywhere in the flow. For a vanishingly small shear rate ($\dot{\gamma} \rightarrow 0$), the apparent viscosity μ_a (Pa·s) approaches the value of $m\tau_y + K(\dot{\gamma})^{n-1}$. This model is used in the present study and the value of m is taken as 100 s throughout. The value of 100 s for m was taken after considerable numerical experimentation starting with $m = 25$ s and going up to $m = 200$ s. For any value of m over 100 s, the flow field virtually stays the same with a great increase in computational time. The diffusion coefficient Γ in the governing equations for u, v, and w is taken equal to the apparent viscosity μ_a. The coupling between the axial velocity component w and the cross-sectional velocity components u and v is established through the variable apparent viscosity.

When curvilinear coordinates $\xi(x, y)$ and $\eta(x, y)$ are introduced, Eqs. 1 and 2 are transformed into

$$\frac{\partial}{\partial\xi}\left[\rho G_1\phi - \frac{\Gamma}{J}\left(\alpha\frac{\partial\phi}{\partial\xi} - \beta\frac{\partial\phi}{\partial\eta}\right)\right] + \frac{\partial}{\partial\eta}\left[\rho G_2\phi - \frac{\Gamma}{J}\left(\gamma\frac{\partial\phi}{\partial\eta} - \beta\frac{\partial\phi}{\partial\xi}\right)\right] = SJ \tag{6}$$

and

$$\dot{\gamma} = \frac{1}{J}\left[2\left(\frac{\partial y}{\partial\eta}\frac{\partial u}{\partial\xi} - \frac{\partial y}{\partial\xi}\frac{\partial u}{\partial\eta}\right)^2 + 2\left(\frac{\partial x}{\partial\eta}\frac{\partial v}{\partial\xi} - \frac{\partial x}{\partial\xi}\frac{\partial v}{\partial\eta}\right)^2 + \left(\frac{\partial y}{\partial\eta}\frac{\partial v}{\partial\xi} - \frac{\partial y}{\partial\xi}\frac{\partial v}{\partial\eta} - \frac{\partial x}{\partial\eta}\frac{\partial u}{\partial\xi} + \frac{\partial x}{\partial\xi}\frac{\partial u}{\partial\eta}\right)^2 + \left(\frac{\partial y}{\partial\eta}\frac{\partial w}{\partial\xi} - \frac{\partial y}{\partial\xi}\frac{\partial w}{\partial\eta}\right)^2 + \left(\frac{\partial x}{\partial\eta}\frac{\partial w}{\partial\xi} - \frac{\partial x}{\partial\xi}\frac{\partial w}{\partial\eta}\right)^2\right]^{1/2} \tag{7}$$

where α, β, γ are the metrics and J is the Jacobian of transformation given by

$$\alpha = \left(\frac{\partial x}{\partial\eta}\right)^2 + \left(\frac{\partial y}{\partial\eta}\right)^2 \tag{8}$$

$$\beta = \frac{\partial x}{\partial\xi}\frac{\partial x}{\partial\eta} + \frac{\partial y}{\partial\xi}\frac{\partial y}{\partial\eta} \tag{9}$$

$$\gamma = \left(\frac{\partial x}{\partial\xi}\right)^2 + \left(\frac{\partial y}{\partial\xi}\right)^2 \tag{10}$$

$$J = \frac{\partial x}{\partial\xi}\frac{\partial y}{\partial\eta} - \frac{\partial x}{\partial\eta}\frac{\partial y}{\partial\xi}. \tag{11}$$

The contravariant velocity components G_1 and G_2 (m/s) are defined as

$$G_1 = u\frac{\partial y}{\partial\eta} - v\frac{\partial x}{\partial\eta} \tag{12}$$

$$G_2 = v\frac{\partial x}{\partial\xi} - u\frac{\partial y}{\partial\xi}. \tag{13}$$

Numerical Procedure

A finite volume algorithm with a nonstaggered grid known as SIMPLEM (a variation of the SIMPLE family of algorithm) proposed by Acharya and Moukalled (1989) is used to analyze the problem. The governing equations are integrated over the control volume cells. Discretization of the integrated equations generates a set of linear algebraic equations of the form

$$a_P\phi_P = a_E\phi_E + a_W\phi_W + a_N\phi_N + a_S\phi_S + b \tag{14}$$

where ϕ is the general variable representing the velocity components or the pressure. The subscript P denotes the nodal point where the variable is calculated and the sub-

scripts E, W, N, and S denote the nodal points east, west, north, and south, respectively, of P. These linearized system of equations for each variable are solved iteratively by a line-by-line successive over-relaxation (LSOR) method. The flow field is solved by a sequential interactive process. Once the velocity field is known (or assumed at the beginning of the iterative process), an improved estimate of the apparent viscosity is obtained from Eq. 4 where the shear stress and shear rate is calculated using Eqs. 5 and 7, respectively. This apparent viscosity is used to solve the velocity and pressure field at the next iteration step. Equation 7 is discretized using a central difference scheme inside the domain and a one-sided forward or backward difference scheme of second-order accuracy at the boundaries. This outer-loop iteration cycle is repeated until

$$\sum_{i,j} \sqrt{\frac{\left(\phi_i^{k+1} - \phi_i^k\right)^2}{\left(\phi_i^k\right)^2}} \leq \epsilon \tag{15}$$

where ϕ is u, v, and w components of velocity, superscripts k and $k+1$ indicate values at two successive iterations, and ϵ is a pre-specified small number.

The boundary conditions on the inner and the outer pipe walls are specified as no slip for the velocities and zero normal gradient for the pressure. The conditions on the other two boundaries in the azimuthal direction (say $i=1$ and $i=i\max$) have to be specified as periodic. The variables at these locations are evaluated from the interior values in such a way that the equality of the variable and its slope at the corresponding boundaries is ensured. This periodicity is imposed by the condition

$$\phi_{1,j} = \frac{\phi_{2,j} + \phi_{i\max-1,j}}{2} = \phi_{i\max,j} \tag{16}$$

where $\phi = G_1$, G_2, w, and p, and $i\max$ is the maximum grid number in the azimuthal direction. The u and v velocity components at these boundaries are determined from the contravariant velocity components G_1 and G_2 as

$$u = \frac{1}{J}\left(G_1\frac{\partial x}{\partial \xi} + G_2\frac{\partial x}{\partial \eta}\right) \tag{17}$$

$$v = \frac{1}{J}\left(G_1\frac{\partial y}{\partial \xi} + G_2\frac{\partial y}{\partial \eta}\right). \tag{18}$$

Usually in the SIMPLEM procedure, the pressure gradient normal to all boundaries is set to zero by setting the corresponding coefficients in the discretized pressure equation to zero. However, at the periodic boundaries, the pressure gradient must not be set equal to zero. This is achieved if the pressure at these boundaries is calculated using Eq. 16, and the corresponding coefficients in the discretized pressure equation are calculated in the usual manner. For the partially blocked case, if the blockage height exceeds the narrow part of the annulus, that is, the narrow part of the annulus is fully blocked (see Figure 2), the flow domain is no longer periodic and this special treatment of the boundary condition is not required.

Results and Discussion

The computations of the helical flow of a yield-power-law fluid are done for both concentric and eccentric annuli. For the purpose of analysis, the following quantities have been used. The radius (m) of the inner cylinder (R_i) and the outer cylinder (R_o) is taken as 0.06 m and 0.12 m, respectively. The fluid considered has a yield stress τ_y of 0.15 Pa and a plastic viscosity K of 0.33 Pa·s^n. Two values of flow behavior index n of 1 and 0.75 have been used. The eccentricity e is defined as $e = d/(R_o - R_i)$ where d is the distance (m) between the centers of the inner and outer cylinders. All calculations are done for a fixed axial pressure gradient $\tilde{P}$ of 25 Pa/m. A counterclockwise rotation of the inner cylinder is assumed. The chosen values for all the parameters above are realistic and typical for drilling conditions. The torque per unit length of the inner cylinder is calculated by summing the product of the tangential component of the shear stress on the inner cylinder surface with the surface area for each control volume cell face on the inner cylinder.

Grid independence study was performed by calculating the total discharge and the torque required to rotate the inner cylinder, while gradually refining the grid in both radial and circumferential directions. It was found that 60×60 grid provides a grid independent solution for all the cases analyzed in the study.

Concentric Annulus

For the concentric annular case with rotating inner cylinder, the flow field is axisymmetric and the flow variation is only in the radial direction.

To date, no analytical solution or experimental data are available for helical flow of yield-power-law fluids in concentric or eccentric annulus. Therefore, for validation purposes, the numerical result for the concentric annulus is compared with the analytical solution of Hanks (1979) for the limiting case of nonrotating inner pipe in Figure 3 which shows excellent agreement for both $n=1$ and 0.75. The radial distance from the inner cylinder surface to the outer cylinder surface is normalized as $R = (r - R_i)/(R_o - R_i)$. The plug-flow zone,

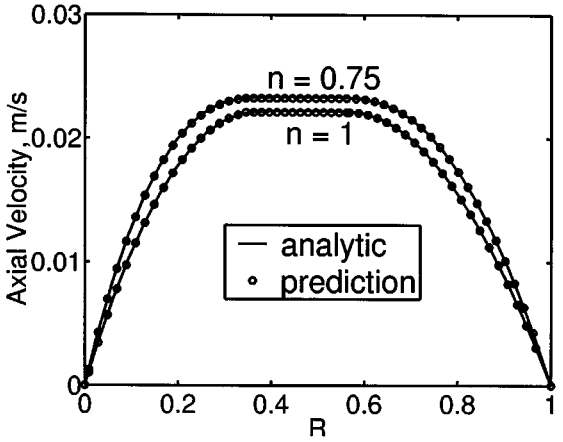

Figure 3. Analytic vs. predicted axial velocity profiles in the annulus for nonrotating concentric inner pipe.

a characteristic feature of fluids having yield stress, is clearly visible in this figure.

The profiles of the axial velocity (m/s) component w in the annulus for different rotational speeds of the inner cylinder ω (rad/s) is presented in Figure 4. It is observed that the axial velocity and, hence, the discharge increases with increasing angular velocity of the inner cylinder. However, this increase is not significant at a higher speed of rotation, especially for $n = 1$. The plug-flow zone diminishes with increasing rotational speed of the inner cylinder. It is also observed that the location of maximum velocity gradually moves towards the inner cylinder with increasing angular speed of the inner cylinder.

The variation of the apparent viscosity μ_a in the annulus for different nonzero values of ω is presented in Figure 5. The resultant shear rate in helical flow is composed of the shear rate due to both axial and tangential flow. For $\omega = 0$, the flow is purely axial and the shear rate near the middle of the annulus becomes very small (axial velocity profile is flatter) which produces large values of μ_a in this region according to Eq. 4. For nonzero ω, additional shear rate due to the tangential flow keeps the resultant shear rate larger, and μ_a increases monotonically from the inner cylinder to the outer cylinder for a particular ω. The total shear rate increases with increasing ω producing the lower values of μ_a at all radial locations in the annulus (see Figure 5). This shear-thinning

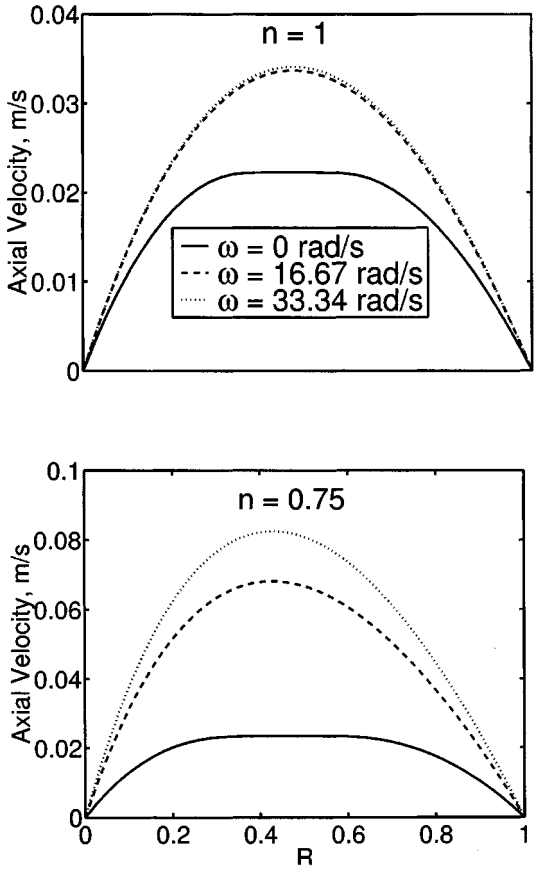

Figure 4. Flow enhancement due to inner pipe rotation for concentric case.

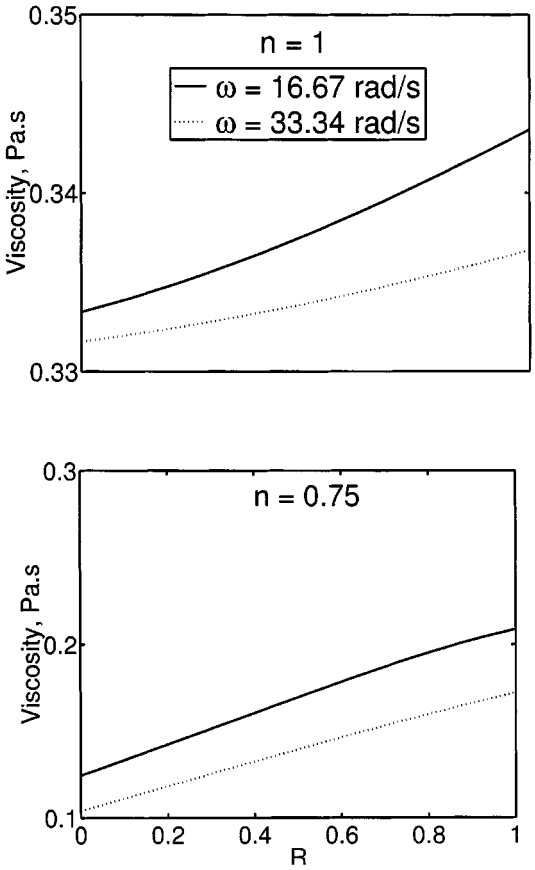

Figure 5. Viscosity profiles in the annulus for concentric case.

with increasing ω leads to an increase in axial-flow rate for a fixed axial pressure gradient.

In reality, the viscosity should not change for Bingham plastic ($n = 1$). However, as shown in Figure 5, there is a small increase in viscosity (~ 2–3%) across the annuli for $n = 1$. This is due to the use of Eq. 5, which is used to handle general viscoplastic fluids of which Bingham plastic ($n = 1$) is a special case. The change in viscosity is significant ($\sim 75\%$) across the annulus when $n = 0.75$.

Eccentric Annulus

As mentioned earlier, the annulus may become eccentric under certain circumstances, especially during directional or inclined drilling. For this reason, it is also important to investigate the effect of the eccentricity on the flow behavior especially on the discharge and torque.

Computations are performed for several values of the eccentricity e and at each eccentricity for two values of the inner cylinder rotational speed ω. As representative cases, the axial velocity distributions, streamlines, and viscosity contours in the annulus with 50% eccentricity and for $\omega = 16.67$ rad/s are shown in Figure 6 for $n = 1$ and 0.75. It is evident from these figures that the velocity is higher in the wide clearance compared to the narrow clearance. Similar behavior was observed for nonrotating inner cylinder in an earlier

work of Hussain and Sharif (1998). The presence of a secondary flow in the wider part of the eccentric annulus is evident from the streamline plots using the u and v velocity components only. There is no secondary flow at low eccentricity, for which the result is not presented. With the increase in eccentricity, secondary flow sets in. For high eccentricity, the secondary flow is more vigorous occupying a significant portion of the annulus. The secondary flow zone is significantly smaller for $n = 0.75$ than for $n = 1$. Significant shear-thinning effect is evident from the viscosity contours for $n = 0.75$ compared to $n = 1$. The viscosity is maximum near the middle of the wider clearance.

The variation of discharge Q with increasing eccentricity is shown in Figure 7 where the discharge is normalized by the corresponding discharge for the concentric case Q_c. For a fixed ω, the discharge rate increases with increasing eccentricity. This behavior is similar to the earlier work of Hussain and Sharif (1998) for nonrotating inner cylinder. This is due to the fact that the increase of flow in the wide part is more than the decrease in the narrow part resulting in a net increase in discharge.

The torque needed to rotate the inner cylinder increases with increasing eccentricity for fixed $\tilde{P}$ and ω as seen in Figure 8 where the torque is normalized by the corresponding torque for the concentric case T_c (N·m). The increasing vigorousness of the secondary flow with increasing eccentricity can be attributed to this increase of the torque requirement.

Similar to the concentric case, the discharge in an eccentric annulus also increases with increasing rotational speed of the inner cylinder due to the shear-thinning effect as pointed

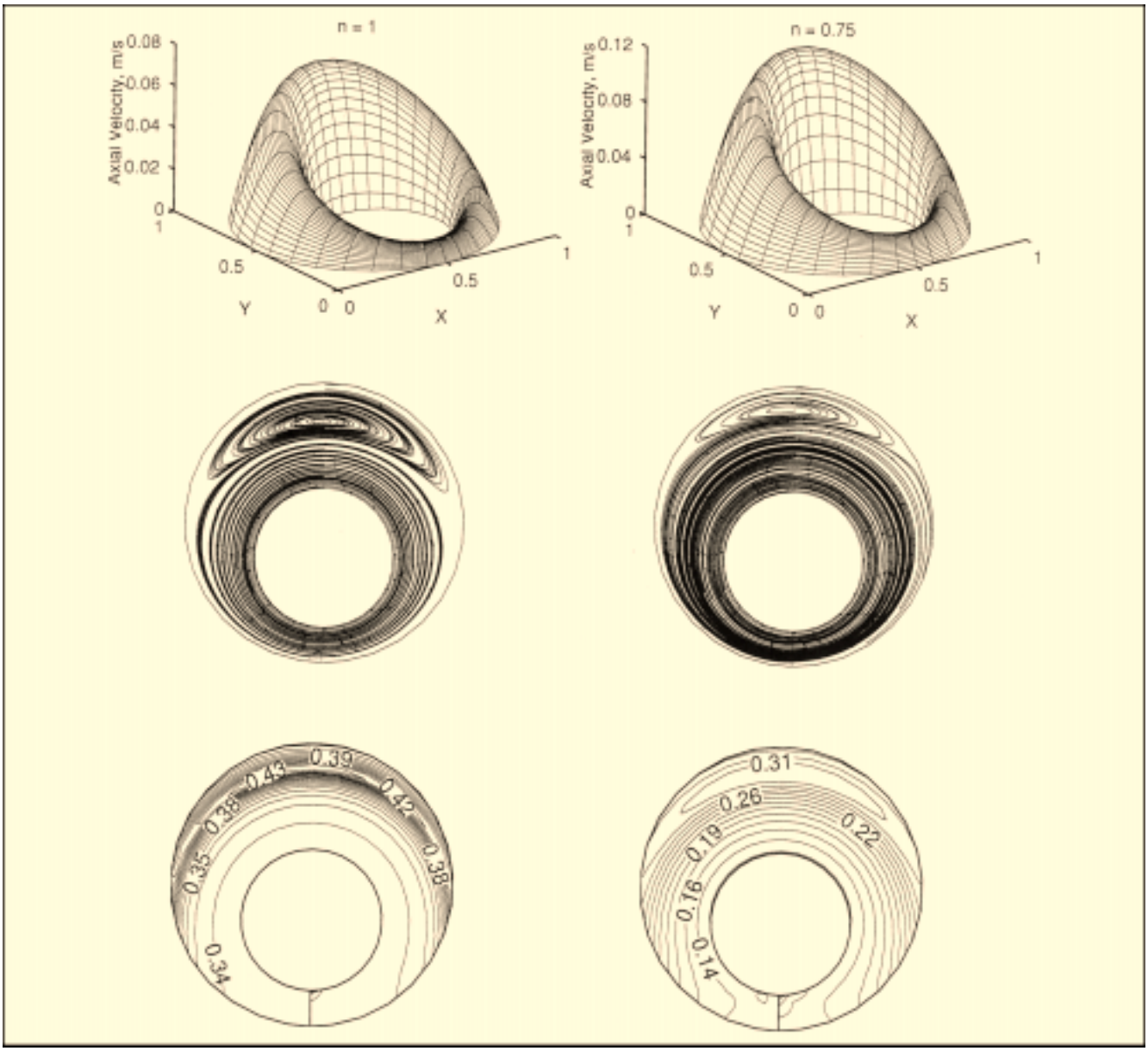

Figure 6. Axial velocity distribution, streamlines, and viscosity contours in the annulus ($\omega = 16.67$ rad/s; $e = 0.5$).

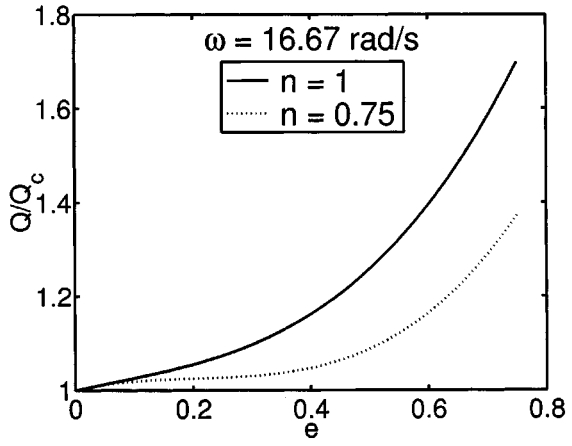

Figure 7. Variation of the discharge with eccentricity.

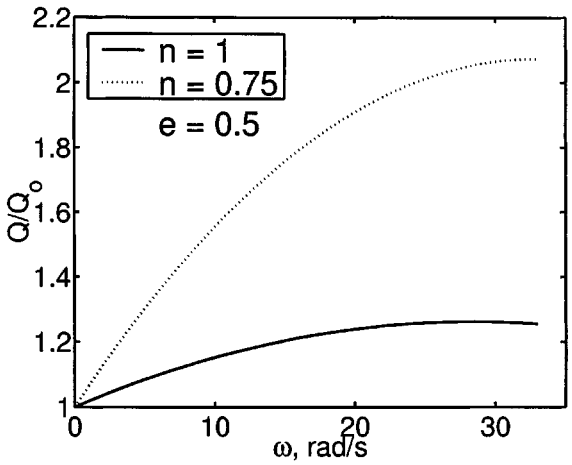

Figure 9. Variation of the discharge with rotational speed of the inner pipe.

out earlier. This is shown in Figure 9 where the discharge is normalized by the corresponding total discharge for nonrotating inner cylinder Q_o.

The effect of axial pressure gradient on the discharge is also investigated. The variation of the discharge with increasing axial pressure gradient is shown in Figure 10 for $\omega = 16.67$ rad/s at 50% eccentricity. As expected, the discharge increases with increasing axial pressure gradient. The rate of increase of discharge is greater for $n = 1$. For viscoplastic fluids, there is no flow for axial pressure gradients below a certain critical value. This critical pressure gradient can be determined through parametric study by gradually lowering the imposed pressure gradient and then extrapolating to the no flow condition. This, however, is not done in this study.

Eccentric Annulus with Blockage

Since the cuttings bed formation in directional drilling is a major problem, the flow in partially blocked eccentric annuli is also investigated using the code. The blockage is imposed on the narrow side of the annulus and the height of the blockage is gradually increased. As mentioned earlier, where this height is greater than the narrow clearance of the annulus, the flow domain is no longer periodic.

The axial velocity profile, streamlines, and viscosity plots for representative cases are presented in Figure 11 when the narrow part of the annulus is partially blocked, and in Figure 12 when the narrow part of the annulus is fully blocked. The flow domain is truncated at the lower end due to the presence of the blockage. A strong secondary flow is found to exist in the wider part of the annulus in these figures.

The variation of the discharge with increasing blockage height is presented in Figure 13 for a representative case. For nonrotating inner pipe, the discharge monotonically decreases with increasing blockage height (Hussain and Sharif, 1998). For rotating inner pipe, however, the discharge is not monotonic, as shown in Figure 13. With a small blockage, discharge is found to decrease similarly to what has been observed with the earlier work with nonrotating inner pipe. With

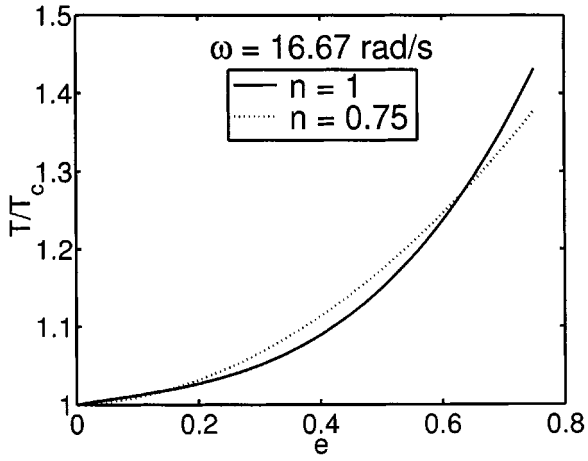

Figure 8. Variation of the torque requirement with eccentricity.

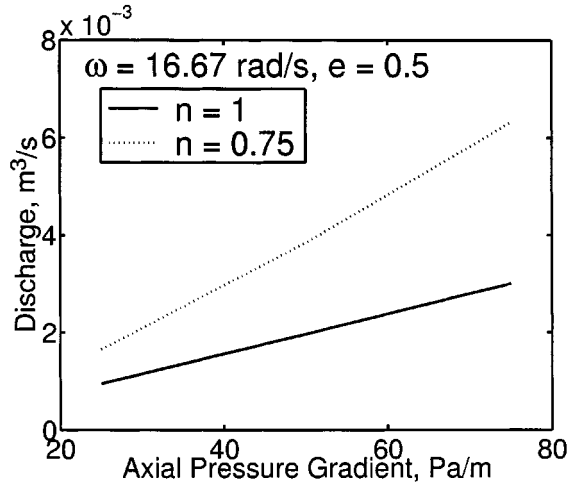

Figure 10. Variation of discharge with axial pressure gradient.

increasing blockage height, the discharge also increases. This phenomenon can be attributed to the fact that the secondary flow in the wider part of the annulus intensifies with increasing blockage height. This results in an increase in shear rate which in turn lowers the viscosity causing the discharge to increase. For even greater blockage height, the flow area is substantially reduced which ultimately results in the lowering of the discharge.

Conclusion

Helical flow of a viscoplastic fluid in concentric and eccentric annuli has been solved numerically using a primitive variable based finite volume algorithm employing nonorthogonal curvilinear coordinates with collocated grids. The fluid is considered to obey the yield-power-law rheological model.

Results show that the axial-flow rate increases with increasing eccentricity and increasing angular velocity of the inner cylinder for the same axial pressure gradient. In an eccentric annulus, a secondary flow zone is present in the wider part of the annulus which intensifies with increasing eccentricity. The torque required to rotate the inner cylinder at a fixed angular velocity also increases with increasing eccentricity. Blockage in the narrow part of the annulus causes the secondary flow to intensify. Discharge is found to decrease, then increase, and then decrease again with increasing blockage height.

The objective of this study was to develop a general numerical model capable of predicting non-Newtonian flow through

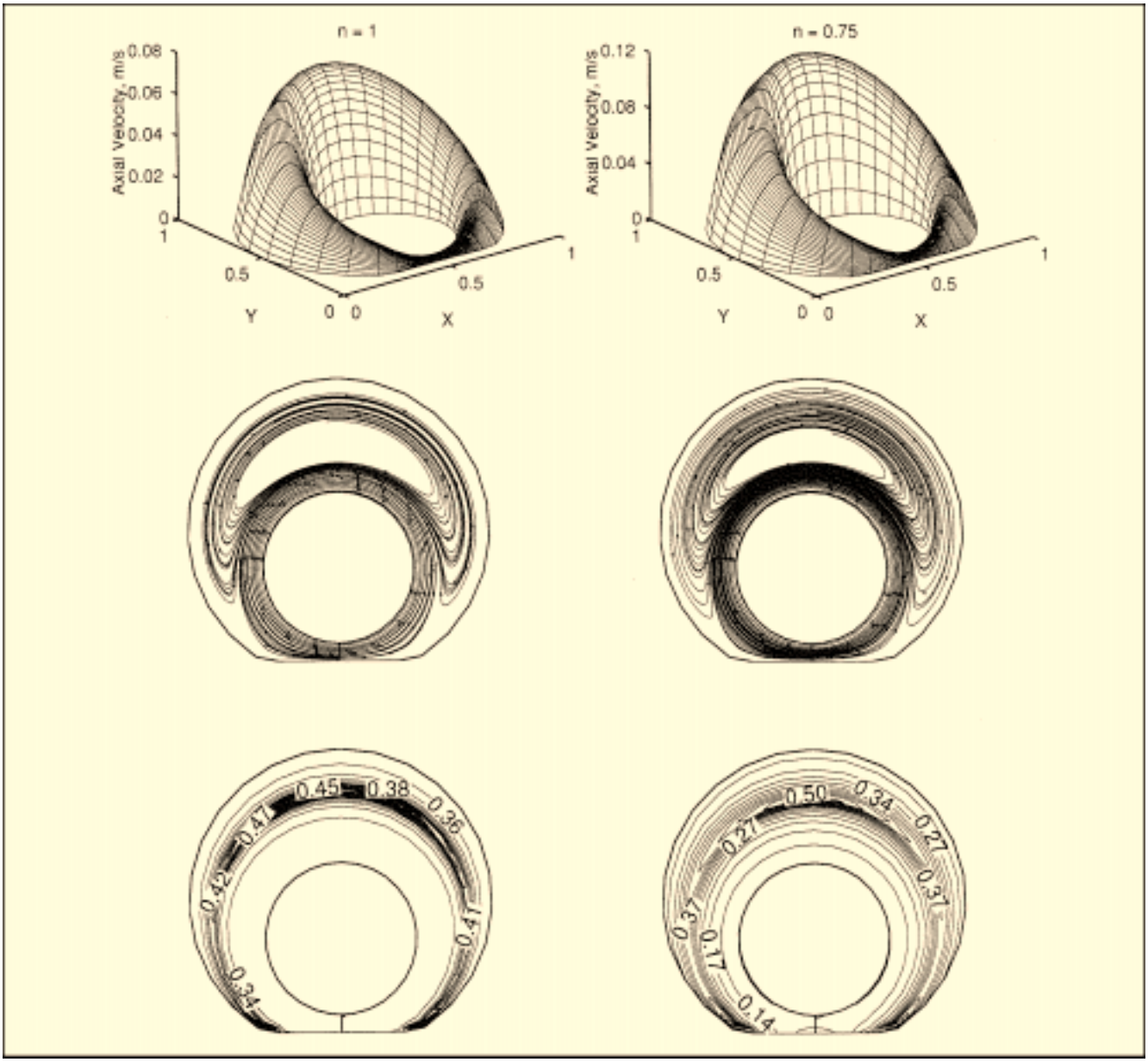

Figure 11. Axial velocity distribution, streamlines, and viscosity contours in the annulus ($\omega = 16.67$ rad/s; $e = 0.5$, $h = 0.016$ m).

irregular eccentric annuli and to use it to produce some useful results. The scope of this study was limited and parametric study encompassing a wide range of rheological parameters and operating conditions could not be performed. As such, the results presented here cannot be generalized.

Acknowledgment

Partial support for this work was provided by William D. Jordan Summer Research Fellowship, Dept. of Aerospace Engineering and Mechanics, The University of Alabama.

Notation

h = blockage height, m
i, j = grid location
Q = flow rate, m^3/s
Q_c = volume flow rate in a concentric annulus, m^3/s
Q_o = volume flow rate with fixed inner cylinder, m^3/s
Q_w = volume flow rate without blockage, m^3/s
r = radial distance, m
R = dimensionless radial distance in a concentric annulus, $(r - R_i)/(R_o - R_i)$
T_o = torque with fixed inner cylinder, N·m
u, v, w = velocity components in the x, y, and z directions, respectively, m/s
x, y, z = Cartesian coordinates
X = dimensionless distance, $x/2R_o$
Y = dimensionless distance, $y/2R_o$
$\dot{\gamma}$ = second invariant of the rate of deformation tensor, 1/s
η, ξ = curvilinear coordinates
ρ = density, kg/m^3

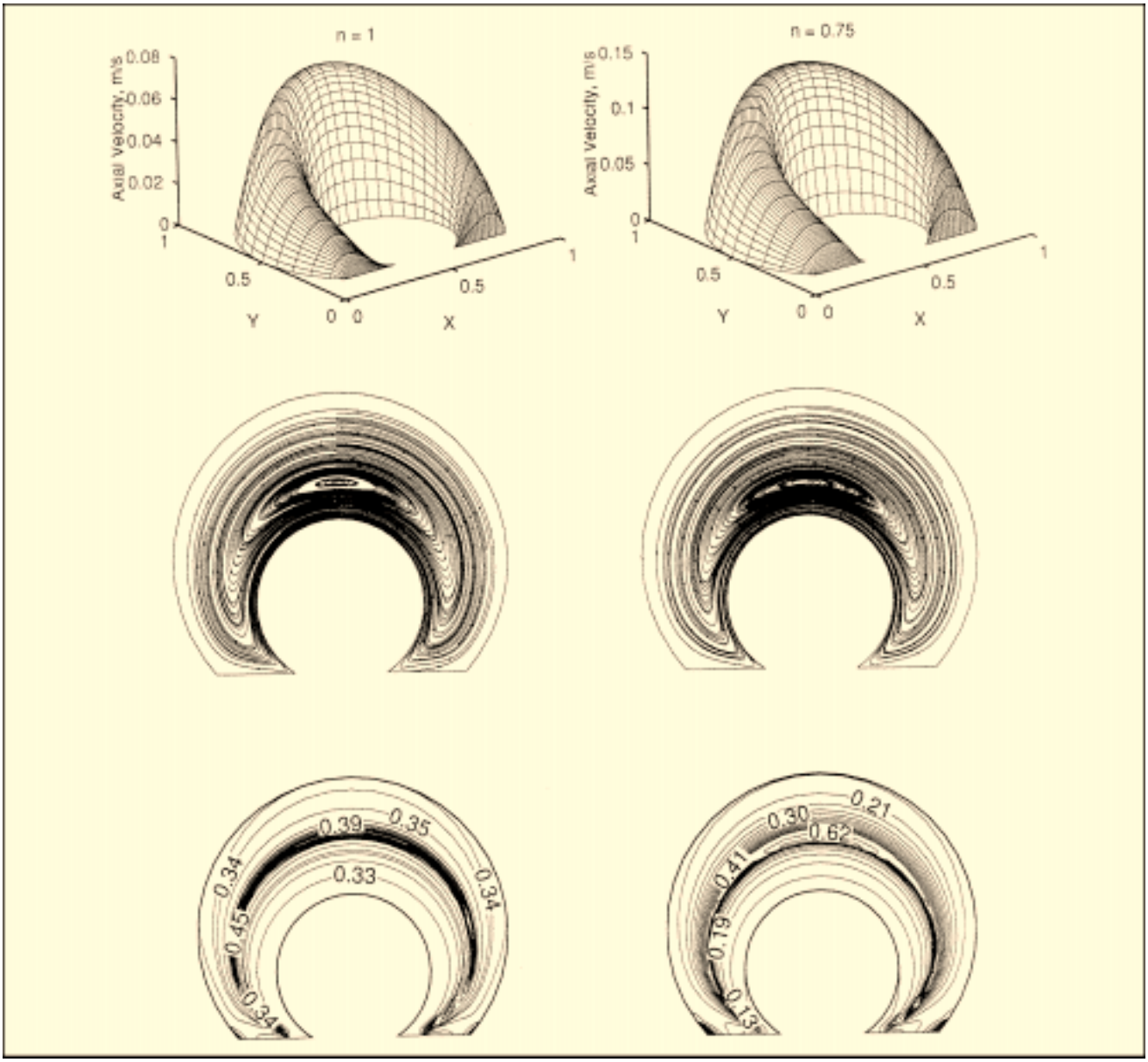

Figure 12. Axial velocity distribution, streamlines, and viscosity contours in the annulus ($\omega = 16.67$ rad/s; $e = 0.5$, $h = 0.04$ m).

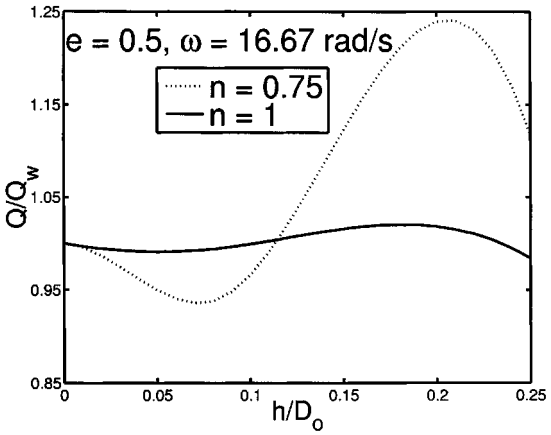

Figure 13. Variation of discharge with blockage height.

Literature Cited

Abdali, S. S., E. Mitsoulis, and N. C. Markatos, ''Entry and Exit Flows of Bingham Fluids,'' *J. of Rheol.*, **36**, 389 (1992).

Acharya, S., and F. H. Moukalled, ''Improvements to Incompressible Flow Calculation on a Non-staggered Curvilinear Grid,'' *Numer. Heat Transf., Part B*, **15**, 131 (1989).

Azouz, I., A. S. Siamack, A. Pilehvari, and J. J. Azar, ''Numerical Simulation of Laminar Flow of Yield-Power-Law Fluids in Conduits of Arbitrary Cross-Section,'' *J. of Fluids Eng.*, **115**, 710 (1993).

Batra, R. L., and M. Eissa, ''Helical Flow of a Sutterby Model Fluid,'' *Poly.-Plastic Technol. and Eng.*, **33**, 489 (1994).

Beverly, C. R., and R. I. Tanner, ''Numerical Analysis of Three-Dimensional Bingham Plastic Flow,'' *J. of Non-Newt. Fluid Mechanics*, **42**, 85 (1992).

Bhattacharya, S. N., and S. H. Javadpour, ''Helical Flow of Herschel Bulkley Fluids,'' *Theoretical and Applied Rheology*, P. Moldenaers and R. Keunings, eds., *Proc. of XI Int. Congress on Rheology*, Brussels, Belgium, p. 896 (Aug. 17–21, 1992).

Bird, R. B., W. E. Stewart, and E. N. Lightfoot, *Transport Phenomena*, Wiley, New York (1960).

Bird, R. B., R. C. Armstrong, and O. Hassager, *Dynamics of Polymeric Liquids*, Wiley, New York (1987).

Coleman, B. D., and W. Noll, ''Helical Flow of General Fluid,'' *J. of Appl. Phys.*, **30**, 1508 (1959).

Cui, H., and X. Liu, ''Research on Helical Flow of Non-Newtonian Fluids in Eccentric Annuli,'' SPE 29940, *Proc. of Int. Meeting on Petrol. Eng.*, Beijing, China, p. 543 (Nov. 14–17, 1995).

Dostál, M., R. Zitný, J. Sesták, and M. Houska, ''Helical Flow of Power-Law Fluids,'' *AIChE J.*, **39**, 189 (Jan., 1993).

Ellwood, K. R., G. C. Georgiou, T. C. Papanastasiou, and O. Wilkes, ''Laminar Jets of Bingham-Plastic Liquids,'' *J. of Rheol.*, **34**, 787 (1990).

Haciislamoglu, M., and J. Langlinais, ''Non-Newtonian Flow in Eccentric Annuli,'' *J. of Energy Res. Technol.*, **112**, 163 (1990).

Hai-Qiao, Z., and W. Ji-Zhou, ''Analytical Solution of the Helical Flow of Non-Newtonian Fluid in Eccentric Annular Space,'' *Appl. Math. and Mechanics*, **15**, Shanghai, China, 657 (1994).

Hanks, W. H., ''The Axial Laminar Flow of Yield-Pseudoplastic Fluids in a Concentric Annulus,'' *Ind. Eng. Chem. Process. Des. Dev.*, **18**, 488 (1979).

Hussain, Q. E., and M. A. R. Sharif, ''Viscoplastic Fluid Flow in Irregular Eccentric Annuli Due to Axial Motion of the Inner Pipe,'' *Can. J. of Chem. Eng.*, **75**, 1038 (1997).

Hussain, Q. E., and M. A. R. Sharif, ''Analysis of Yield-Power-Law Fluid Flow in Irregular Eccentric Annuli,'' *J. of Energy Res. Technol.*, **120**, 201 (1998).

Mitsoulis, E., S. S. Abdali, and N. C. Markatos, ''Flow Simulation of Herschel-Bulkley Fluids through Extrusion Dies,'' *Can. J. of Chem. Eng.*, **71**, 147 (1993).

Papanastasiou, T. C., ''Flow of Materials with Yield,'' *J. of Rheol.*, **31**, 385 (1987).

Pham, T. V., and E. Mitsoulis, ''Entry and Exit Flows of Casson Fluids,'' *Can. J. of Chem. Eng.*, **72**, 1080 (1994).

Vradis, G. C., J. Dougher, and S. Kumar, ''Entrance Pipe Flow and Heat Transfer for a Bingham Plastic,'' *Int. J. of Heat and Mass Transf.*, **36**, 543 (1993).

Wei, X., S. Z. Miska, N. E. Takach, P. Bern, and P. Kenny, ''The Effect of Drill-Pipe Rotation on Annular Frictional Pressure Loss,'' *J. of Energy Res. Technol.*, **120**, 61 (1998).

Manuscript received Sept. 9, 1999, and revision received Apr. 24, 2000.